Delayed detection of climate mitigation benefits due to climate inertia and variability

Claudia Tebaldi[a,1] and Pierre Friedlingstein[b]

[a]Climate Central and National Center for Atmospheric Research, Boulder, CO 80307; and [b]College of Engineering, Mathematics, and Physical Sciences, University of Exeter, Exeter EX4 4QJ, United Kingdom

Edited by Benjamin D. Santer, Lawrence Livermore National Laboratory, Livermore, CA, and approved September 6, 2013 (received for review January 1, 2013)

Climate change mitigation acts by reducing greenhouse gas emissions, and thus curbing, or even reversing, the increase in their atmospheric concentration. This reduces the associated anthropogenic radiative forcing, and hence the size of the warming. Because of the inertia and internal variability affecting the climate system and the global carbon cycle, it is unlikely that a reduction in warming would be immediately discernible. Here we use 21st century simulations from the latest ensemble of Earth System Model experiments to investigate and quantify when mitigation becomes clearly discernible. We use one of the scenarios as a reference for a strong mitigation strategy, Representative Concentration Pathway (RCP) 2.6 and compare its outcome with either RCP4.5 or RCP8.5, both of which are less severe mitigation pathways. We analyze global mean atmospheric CO_2, and changes in annually and seasonally averaged surface temperature at global and regional scales. For global mean surface temperature, the median detection time of mitigation is about 25–30 y after RCP2.6 emissions depart from the higher emission trajectories. This translates into detection of a mitigation signal by 2035 or 2045, depending on whether the comparison is with RCP8.5 or RCP4.5, respectively. The detection of climate benefits of emission mitigation occurs later at regional scales, with a median detection time between 30 and 45 y after emission paths separate. Requiring a 95% confidence level induces a delay of several decades, bringing detection time toward the end of the 21st century.

regional climate change | climate variability | signal detection

The Fifth Assessment Report of the Intergovernmental Panel on Climate Change states, in its summary for policy makers, that "Warming of the climate system is unequivocal" and that "It is extremely likely that human influence has been the dominant cause of the observed warming since the mid-20th century" (1). To drive simulations of future climate, phase 5 of the Coupled Model Intercomparison Project (CMIP5) (2) prescribed a new set of four scenarios, the Representative Concentration Pathways (RCPs), describing future emissions of major greenhouse gases and aerosol precursors (3, 4). These four RCPs span the range of radiative forcing found in the existing integrated assessment model literature and lead to global radiative forcing levels of about 2.6, 4.5, 6.0, and 8.5 watts per square meter (Wm^{-2}) by the end of the 21st century. Starting from present-day (year 2005) concentrations, the scenarios diverge, three of them within the next two decades. By 2100, it is estimated that CO_2 emissions will range from 29 petagrams of carbon per year (PgCyr-1) for RCP8.5 to –0.5 PgCyr-1 for RCP2.6 (5) (Fig. 1).

RCP2.6 assumes implementation of strong climate mitigation policies, aiming to limit global warming to less than 2 °C relative to the estimated preindustrial temperature. Compared with less stringent mitigation scenarios, such as the two medium stabilization scenarios (RCP4.5 and RCP6.0) or the much higher unmitigated emission scenario (RCP8.5), the benefits in terms of avoided climate change would be significant. By 2100, models simulate global surface warming of around 2 °C above preindustrial level under RCP2.6 and show warming of about 5 °C under RCP8.5 (6, 7). These benefits would be achieved only with full participation of all countries in a stringent emission reduction program, substantial changes in energy use, and intensive use of carbon capture and storage and biofuels, with the estimated cost of abating greenhouse gas emissions reaching 1.7% of the global gross domestic product by 2050 (8).

However, the long lifetime of atmospheric CO_2, combined with the large inertia of the climate system due to the slow mixing of heat in the ocean, means that the near-surface temperature warming rates will not immediately decline even if greenhouse gas emissions drop rapidly, as in RCP2.6. Furthermore, internal modes of variability on a range of space and time scales (from interannual to multidecadal) could hamper early detection of the underlying climate signals arising from different mitigation decisions. If these delays in the effects of mitigation are not understood as only temporary, they could arguably challenge the continuation of global efforts in curbing anthropogenic emissions. Our study aims at characterizing and quantifying these temporary delays, by detecting the time at which the mitigation-induced climate change signal emerges from the noise of internal variability. We see the results as not only interesting in a scientific perspective, because this study quantifies such waiting times and their uncertainty at both global and regional scales, but also relevant to policy making, because they inform the public and decision makers that (otherwise frustrating) time delays should be expected.

The concept of detection is used in climate science when identifying the long-term historic changes in climate variables (9) that cannot be explained by internal variability alone. Here, we extend it, as in other recent studies (10, 11), to detecting the emergence of a signal in future climate simulations, specifically

Significance

One of the benefits of climate mitigation policies is the reduction of future warming. Here, we estimate the time at which we can detect the mitigation signal arising from reducing future emissions of greenhouse gases. Estimation of detection time is inherently a signal-to-noise issue, requiring consideration of uncertainties in both internal variability and model responses to anthropogenic influences. We provide detection times in terms of best estimates and uncertainty ranges. Our study addresses the critical question of how long we may need to wait until we can clearly identify the benefits (in terms of avoided warming) of different mitigation pathways. This question is not only of scientific relevance, but it is also of direct concern to policymakers and the public.

Author contributions: C.T. and P.F. designed research; C.T. and P.F. performed research; C.T. analyzed data; and C.T. and P.F. wrote the paper.

The authors declare no conflict of interest.

This article is a PNAS Direct Submission.

[1]To whom correspondence should be addressed. E-mail: ctebaldi@climatecentral.org.

This article contains supporting information online at www.pnas.org/lookup/suppl/doi:10.1073/pnas.1300005110/-/DCSupplemental.

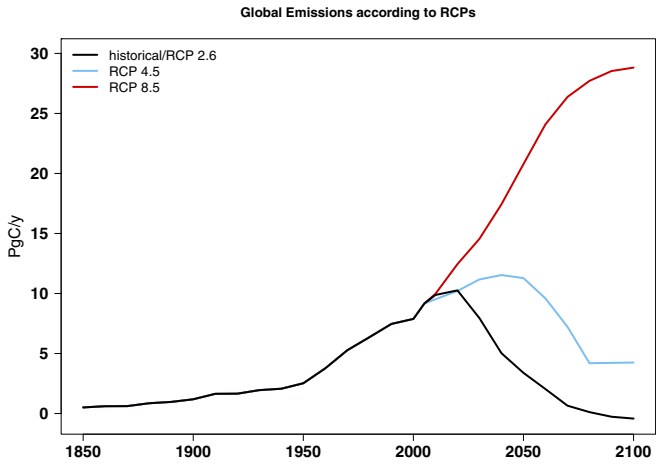

Fig. 1. CO_2 emission pathways according to historical estimates and RCP assumptions.

in global CO_2 atmospheric concentrations and average surface air temperatures (TAS) over the 21st century. In our study, the signal is that of mitigation, as we ask at what time its benefits, in terms of lower CO_2 concentrations and lower atmospheric temperatures, will become detectable from the background noise. The problem of detecting mitigation benefits therefore sets our detection problem apart from the traditional detection of a signal in individual scenario experiments (12). We argue that the effects of mitigation can only be defined in relative terms, as the emergence of a significant difference between the characteristics of a world under mitigation and those of the world that might have been in its absence.

The sources of uncertainty affecting the identification of the emerging signal can be identified in (*i*) the confounding effect of internal, high-frequency variability and, most importantly, for the detection of a long-term trend, low-frequency variability; (*ii*) the unknown amplitude of these internal modes; and (*iii*) the unknown value of climate sensitivity, determining the strength of the climate system response to external forcing. We design the study to address all three sources:

i) We seek to minimize the confounding effect of multidecadal noise by defining the signal of mitigation as a statistically significant trend emerging in the yearly values of a time series of differences between the output (CO_2 or TAS) of climate model simulations under the RCP2.6 scenario and the corresponding output under a counterfactual scenario (RCP4.5 or RCP8.5). Using yearly differences between scenarios should dampen the low-frequency variability of the two original time series and, correspondingly, should let high-frequency variability be the major determinant of the correlation structure of the resulting time series. We empirically estimate the correlation structure of the difference series and account for it in the statistical noise model.

ii) We perform the differencing between mitigation and counterfactual scenarios using multiple initial-condition ensemble members (ICs) within each of five different climate models to explore the effect of different realization of internal variability but also expecting the size of internal variability to be different across the five models. By considering the set of within-model results, our summary estimates should be robust to the form and size of the internally generated noise.

iii) Finally, we also take between-scenario differences by pairing individual time series from different climate models, thus letting the different sizes of internal variability (11); climate sensitivity; and, more generally, model structural uncertainty (13, 14) combine to confound the signal further in this between-model approach.

We propose this latter method, differencing across models, not simply as a stress test of the robustness of our quantitative estimates. In addition, we mimic through this approach a real-world situation whereby, having pursued a mitigation policy, the question could be raised of how large a benefit it provided. The answer could only be obtained by comparing the real-world temperature outcomes with modeled temperatures under counterfactual scenarios; however, in the presence of uncertainty about climate sensitivity, a range of models would have to be used. Taking this thought exercise one step further, as we stand here today imagining this future test, we do not know what the mitigation outcome will be either; hence, the necessity of performing this analysis across a set of models by pairing them in all possible combinations.

We use five Earth System Models (ESMs) from CMIP5 (2) that span a range of equilibrium climate sensitivity (15) between 2.7 °C and 4.6 °C, and provide at least three ICs for the three RCPs of interest (RCP2.6, RCP4.5, and RCP8.5, diverging in their emission paths by 2020 at the latest; Fig. 1) (3). Table S1 describes the relevant characteristics of the five ESMs.

In essence, we seek to determine when (*i*) annual difference values of atmospheric CO_2 concentration and TAS between a nonmitigation scenario and the "baseline" RCP2.6 mitigation scenario start showing a significant trend and (*ii*) the emergence of this trend from the year-to-year noise is established permanently for the remaining length of the simulations considered. We analyze time series of global averages for CO_2 and TAS, as well as regional averages of TAS, using the Coordinated Regional climate Downscaling Experiment (CORDEX) domains (16) (averaging TAS over land only) shown in Fig. 2. We also analyze seasonal values of TAS (boreal winter [December-January-February (DJF)] and boreal summer [June-July-August (JJA)]). A further description of our statistical approach is provided in *Materials and Methods*, and details are provided in *SI Text*.

Results for CO_2 Concentrations

First, we apply the within-model type of analysis to time series of CO_2 concentrations from different RCPs. To the scenario-specified time series of CO_2 concentration, we superimpose variability derived for each of the three ICs by estimating the Institut Pierre-Simon Laplace coupled model version 5A lower resolution (IPSL-CM5A-LR) model's land fluxes over seasonal and interannual time scales (Fig. 3, *Upper*; concentration trajectories). The year-to-year variability (the standard deviation of the yearly values after detrending the time series) is on the order of a unit (parts per million), and it disappears on the scale of total concentration values. Because atmospheric CO_2 concentration is proportional to cumulative emissions, sustained significant emission reduction leads to atmospheric concentration rapidly separating, dwarfing the natural year-to-year variability, and the trend in the time series of differences emerges as significant very quickly (Fig. 3, *Lower*) as a result of a large signal-to-noise ratio in atmospheric CO_2 concentrations (17, 18) (on the order of 60–130 to 450 depending on the scenario considered; Table S1). Times to detection are consistently on the order of 10 y from the time of separation of the CO_2 emission pathways (Table 1). We expect the results from IPSL-CM5A-LR to be very similar for other ESMs because the high signal-to-noise ratio is a characteristic common to the carbon cycles of all ESMs (19).

Results for Global, Regional, and Seasonal Temperatures

How much longer does it take for the effect of mitigation on temperatures to become apparent? We analyze 21st century time series of annual and seasonal values of TAS at global and

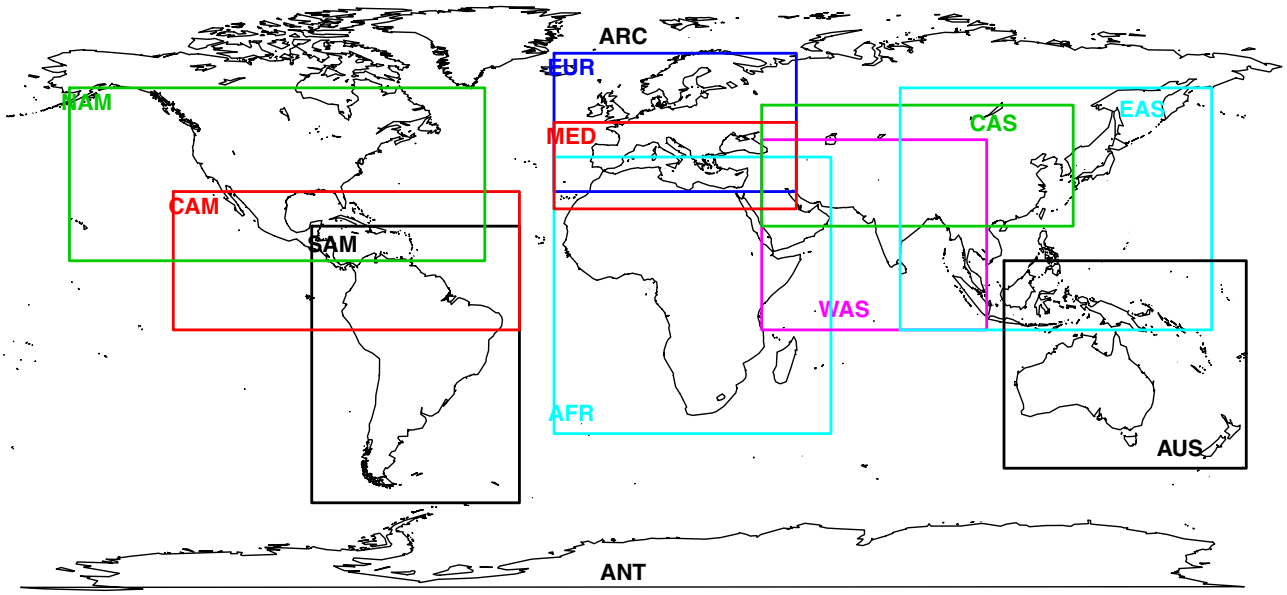

Fig. 2. The 12 regional domains over which we average model output of TAS at annual and seasonal (DJF and JJA) scales, in addition to considering global averages (global average and global land-only average). The regions are Africa (AFR), Antarctica (ANT), Arctic (ARC), Australia (AUS), Central America (CAM), Central Asia (CAS), East Asia (EAS), Europe (EUR), Mediterranean Basin (MED), North America (NAM), South America (SAM), and Western Asia (WAS).

regional scales [averaging TAS over the CORDEX land-only domains (16); Fig. 2].

For each individual global, regional, and seasonal or annual average, the individual IC trajectories of TAS from different RCPs eventually separate over the course of the future period [e.g., Fig. 4, *Upper*; time series of globally averaged TAS from three ICs of one of the models, Community Climate System Model version 4 (CCSM4), using historical forcings (1850–2005), followed by the three RCPs (2006–2100); corresponding plots for the other four ESMs considered are shown in Fig. S1]; thus, we expect that yearly differences between any IC under RCP2.6 and any IC under a higher scenario will eventually show a significant trend [Fig. 4, *Lower*; two corresponding sets of nine trajectories of yearly differences between any IC from the two counterfactual scenarios, RCP4.5 (light blue) and RCP8.5 (red), and any IC from RCP2.6]. We expect the noise in the trajectories of these differences to be confounding at first, but after a few decades, we expect a significant and persistent positive trend to emerge. Individual trajectories differ in the exact year when the trend emerges. As described in *Material and Methods*, we compute 225 values of the time of emergence of a significant and lasting positive trend for each of the two "mitigation vs. counterfactual scenarios" choices. To validate our methodology in a fashion as close as possible to detection and attribution approaches, we apply the same analysis to the time series of differences between ICs under the same scenario, which constitute for us "control" cases. We never find a case where a significant trend emerges and persists in these control cases. We take this result as further supporting the robustness of our detection estimates, because it confirms that no trend from the convolution of multidecadal

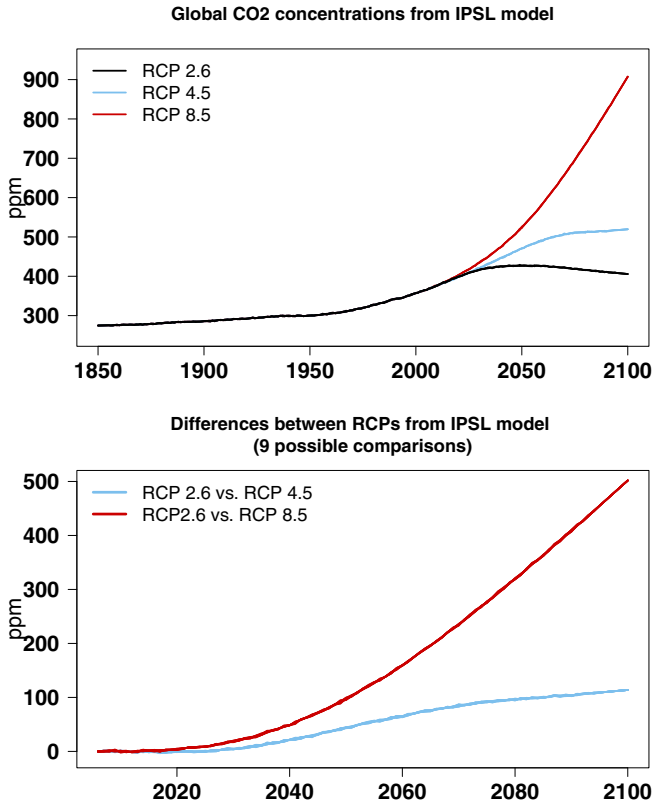

Fig. 3. Atmospheric CO_2 concentration time series (*Upper*) and their differences (*Lower*) obtained from the IPSL-CM5A-LR model (three ICs for each scenario).

Table 1. Time to detection of mitigation when analyzing differences in annual values of CO_2 concentrations from IPSL-CM5A-LR

IPSL-CM5A-LR	RCP2.6 vs. RCP4.5	RCP2.6 vs. RCP8.5
1 ensemble member	2030 (10)	2019 (9)
5 ensemble members	2031 (11)	2021 (11)
9 ensemble members	2031 (11)	2022 (12)

The variability is modeled on the basis of the ESM's seasonal land fluxes. Values are listed as calendar year and, in parentheses, as number of years since the separation of emission paths under the two counterfactual RCPs considered.

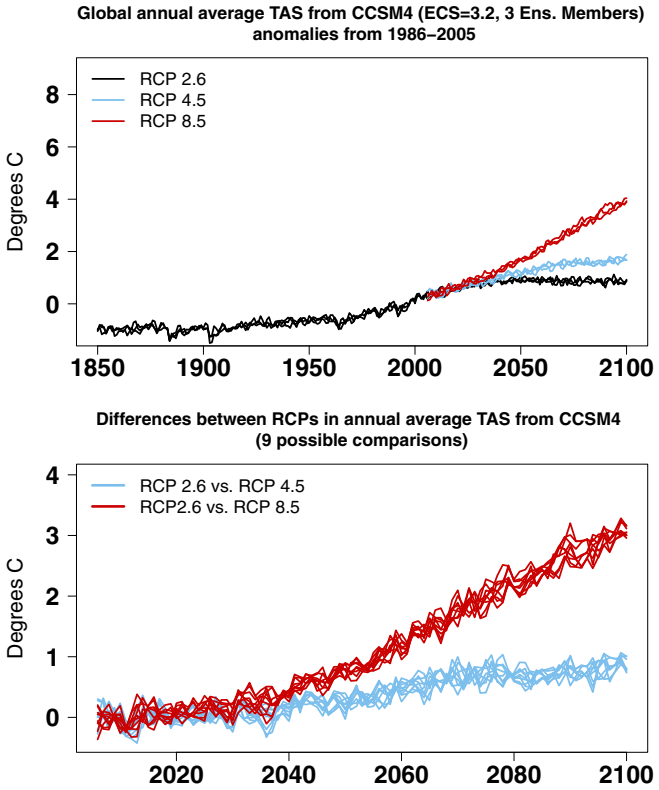

Fig. 4. (*Upper*) Time series of globally averaged (GLO) annual mean value of TAS for the historic period and three RCPs as simulated by one ESM (CCSM4); each line represents an individual ensemble (Ens.) member. (*Lower*) Time series of year-by-year differences in global average annual temperatures between each combination (total of nine) of ensemble members, as represented in *Upper*, under the two pairs of RCPs, RCP8.5 vs. RCP2.6 (red) and RCP4.5 vs. RCP2.6 (light blue).

variability, which would affect these within-scenario differences as well as the between-scenarios differences, emerges and persists. Note, however, that this "sanity check" can be performed only within models, because the differences between models could be affected by differences in the response due to climate sensitivity, which could introduce systematic trends even for differences taken under the same scenario.

The comparison across regions confirms, as expected, that detection happens earlier at global than regional scales and when both ocean and land domains are averaged, thanks to a larger signal-to-noise ratio over oceans. When using RCP4.5, median times to detection start around 2045 at the global scale (25–30 y after the separation of the CO_2 emissions paths between these two scenarios) and as late as 2060 for annual averages over some regions (Australia or Antarctica) (Table 2). Generally, winter averages (DJF in the Northern Hemisphere, JJA in the Southern Hemisphere) are more challenging for detection, adding, on average, a decade to the detection time, whereas summer averages behave similar to annual averages (Tables S2 and S3). This is mainly due to a larger variability (noise) in the wintertime TAS that more than makes up for a slightly larger signal in the same seasonal values. As an example, for North America averages under the RCP4.5 comparison, representing the regional results showing the larger difference in detection time statistics between annual and summer averages, on the one hand, and winter averages, on the other hand, the noise size is two- to threefold larger in winter (depending on the ESM), whereas the signal is only a fraction (10–15%) larger in that season. The spread of times to detection is very wide, covering about five decades in most cases. For globally averaged temperature, detection at a 95% confidence level only happens around 2075 when using RCP4.5, which is 55 y after the emission paths diverge. Fig. 5 summarizes these results for global and regional TAS (annual and seasonal averages) from the comparison between RCP2.6 and either RCP4.5 (*Upper*) or RCP 8.5 (*Lower*). We add along the right axis time defined in years after separation of emission pathways.

The most striking difference when using RCP8.5 as counterfactual pertains to the width of the distributions rather than their medians, when considering that the CO_2 emission pathways of RCP2.6 and RCP8.5 diverge 10 y earlier (around 2010) than for RCP2.6 and RCP4.5. The ranges of the distributions in Fig. 5 (*Lower*) are significantly narrower, because natural variability plays a relatively lesser role in the presence of a stronger anthropogenic signal. The fifth to 95th percentile span, on average, three decades rather than five decades, with a detection at the

Table 2. Statistics from the distributions of times of detection obtained across 225 differences for each of two comparisons (RCP2.6 vs. RCP4.5 and RCP2.6 vs. RCP8.5)

RCP2.6 vs. RCP4.5				RCP2.6 vs. RCP8.5			
Region	Fifth percentile	Median	95th percentile	Region	Fifth percentile	Median	95th percentile
GLO	2022 (2)	2045 (25)	2077 (57)	GLO	2021 (11)	2037 (27)	2055 (45)
LAND_GLO	2027 (5)	2047 (27)	2074 (54)	LAND_GLO	2022 (12)	2039 (29)	2053 (43)
WAS	2031 (11)	2050 (30)	2079 (59)	AFR	2024 (14)	2041 (31)	2054 (44)
AFR	2032 (12)	2051 (31)	2085 (65)	WAS	2026 (16)	2041 (31)	2053 (43)
CAS	2029 (9)	2051 (31)	2076 (56)	MED	2028 (18)	2042 (32)	2057 (47)
NAM	2029 (9)	2051 (31)	2080 (60)	CAS	2029 (19)	2043 (33)	2057 (47)
EAS	2031 (11)	2052 (32)	2074 (54)	EAS	2028 (18)	2043 (33)	2057 (47)
ARC	2028 (8)	2054 (34)	2082 (62)	ARC	2025 (15)	2044 (34)	2058 (48)
CAM	2032 (12)	2054 (34)	2086 (66)	NAM	2028 (18)	2045 (35)	2059 (49)
SAM	2033 (13)	2054 (34)	2086 (66)	AUS	2031 (21)	2046 (36)	2061 (51)
EUR	2037 (17)	2055 (35)	2088 (68)	CAM	2028 (18)	2046 (36)	2065 (55)
MED	2035 (15)	2056 (36)	2084 (64)	SAM	2029 (19)	2046 (36)	2065 (55)
AUS	2039 (19)	2058 (38)	2089 (69)	EUR	2031 (21)	2047 (37)	2060 (50)
ANT	2042 (22)	2064 (44)	2097 (77)	ANT	2033 (23)	2051 (41)	2075 (65)

Values are listed as calendar year and, in parentheses, as number of years since the separation of emission paths under the two counterfactual RCPs considered. AFR, Africa; ANT, Antarctica; ARC, Arctic; AUS, Australia; CAM, Central America; CAS, Central Asia; EAS, East Asia; EUR, Europe; GLO, global average; LAND_GLO, global land-only average; MED, Mediterranean Basin; NAM, North America; SAM, South America; WAS, Western Asia.

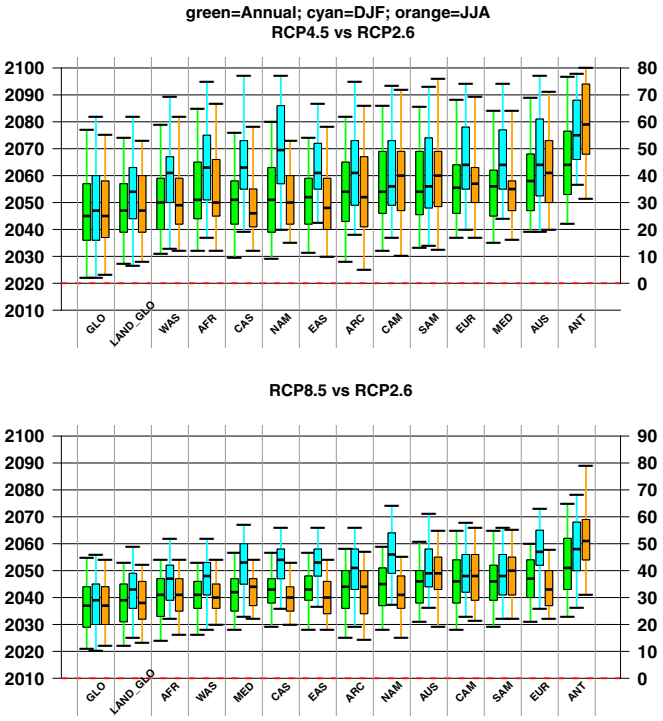

Fig. 5. Distributions of time of detection for global and regional temperatures, using RCP2.6 as a baseline and RCP4.5 (*Upper*) or RCP8.5 (*Lower*) as a counterfactual scenario. For each regional domain, three distributions are summarized by box plots, with one pertaining to annual average TAS (*Left*, green), one for DJF average TAS (*Center*, cyan), and one for JJA averages (*Right*, orange). Each box plot shows the median of the distribution as a thick line within the box and the interquartile range as the lower and upper sides of the box. The whiskers extend from the fifth quantile to the 95th quantile. Regions are ordered by increasing median detection time using annual average TAS results (green box plots, thick lines). The red line marks the time of clear separation in the CO_2 emission pathways of the two scenarios. The axis to the right measures the time of detection in terms of years since the separation in emission pathways has occurred.

95% confidence level around 2055 for global annual temperature, 45 y after emission paths diverge rather than 55 y as in the case for RCP4.5.

The large uncertainty in detection times, up to 60 y for RCP4.5 vs. RCP2.6, results from the combination of time series from models with different climate sensitivity and signal-to-noise characteristics. Fig. S2 and Table S4 show how much narrower ranges would be for global TAS when performing this analysis within each individual model. In reality, model uncertainty, together with uncertainties about the size of low-frequency internal variability, compound to determine the waiting times quantified here.

Results may vary even more significantly when using smaller and better separated domains, such as, for example, the regions of Giorgi and Francisco (20) (Fig. S3).

Discussion

We have performed a detection analysis of the times until the effects of future mitigation over global atmospheric CO_2 concentrations and annual and seasonal surface temperatures become significant at the global scale and, for temperature, also at the regional scale, accounting for the sensitivity of results to model uncertainties, internal variability, and the strength of the signal under the counterfactual nonmitigation scenario. We find a wide range of results but, as a consensus estimate, for temperature, time to detection is not shorter than 25 y after emission mitigation starts, even using the median of the distribution as the criterion. The median time to detection, relative to the time of departure of emissions, is not significantly reduced when comparing RCP2.6 with RCP8.5, but the range of outcomes, and therefore the uncertainty, is significantly so. These numbers apply to global average temperature, and they increase when considering regional outcomes, on average, by 5–10 y. The signal-to-noise ratio for CO_2 concentrations over time is at least an order of magnitude larger than for surface temperatures; hence, the separation of concentration pathways is detectable much earlier and more robustly within about 10 y from the emission separation. This indicates that the absence of early discernibility of the climate benefits of mitigation is due to the inertia and internal variability of the physical climate system rather than the global carbon cycle.

As studies using the more traditional detection and attribution methodologies have shown, large-scale average temperatures most readily reveal the fingerprint of external forcings (21); thus, we expect detection of benefits relevant to other climate variables to be even further delayed. We expect those variables related to temperature averages (e.g., atmospheric temperatures, heights, thicknesses) to show similar times to detection, whereas other variables with smaller signal-to-noise ratios, such as precipitation or other aspects of the hydrological cycle and extremes, are expected to show delay in detection of mitigation. Recently, using a simple model tuned to reproduce CCSM4 climate sensitivity, the behavior of sea level rise under different mitigation scenarios was analyzed (22), focusing on the effects of mitigation of short-lived species as opposed to the more traditional CO_2 mitigation pathways that we address here. That analysis suggests that CO_2 mitigation effects on sea level rise compared with a business as usual scenario are further delayed compared with changes in global temperatures, and the effects would not be perceivable until well into the second half of this century. The scenarios used in that analysis are RCP2.6 for the CO_2 mitigation case and RCP 6.0 for "business as usual."

Our results use CO_2 emissions as a measure of global mitigation but would be very similar if using total greenhouse gases forcing (5). Sulfate aerosols do not affect these results because their emissions decrease at similar rates in all RCP scenarios (4).

Times to detection appear long under a naive expectation that climate impact of mitigation action would be discernible immediately. From the opposite perspective, our results suggest that the benefits would be apparent in all cases before the end of this century, and even by the middle of the century in many regions.

Materials and Methods

Because we look to detect a signal in a time series of annual differences between two original time series of model output, we are dealing with noise larger in amplitude than if we were concerned with detecting a signal in the original time series (similar to what we would have accounted for had we considered the emergence of significant trends in the individual time series first and then tested the hypothesis that these trends differed from one another). Also, because computing year-by-year differences changes the spectral characteristics of the resulting series compared with the original two series, we are not necessarily affected by decadal or multidecadal internal variability with the same characteristics as the original time series; neither we can simply sum the variability of the two original time series, because they may not be mutually independent. Therefore, we proceed through a purely empirical analysis of the difference time series as follows. Each of our trend analysis consists of fitting linear models by generalized least squares using years as the predictor. Generalized least squares compute estimates of the coefficients of a regression by using estimates of the covariance matrix of the residuals that account for the presence of time correlation (the algorithm is usually implemented as a recursive estimation). Accounting for time correlation in the residuals does not usually change the estimated value of the linear coefficient (the trend value in our case) significantly but increases the estimated value of its variance, which crucially affects the outcome of any test of significance. For our difference time series, we find that an autoregressive structure of order 1 (AR1) is appropriate to account for the temporal autocorrelation of the residuals in all cases. Therefore, our trend estimates and significance testing are based on the generalized least squares fit of the time

series, with an estimate of the covariance matrix of the residuals obtained by fitting the parameters of an AR1 process to them. The estimation procedure is automatically performed, once the order of the AR process is specified, in, for example, the implementation of the function gls() in the software package R (www.R-project.org/).

Trend analysis is performed on all possible time series of year-by-year differences obtained by comparing each of the 15 members of RCP2.6 simulations with each of the 15 members of RCP4.5 or RCP8.5 simulations (model output is first averaged over the regional domains and into annual or seasonal means). Trends over increasingly long stretches of the time series (10-, 11-, 12-,...95-y long stretches starting at 2005) are computed and tested for significance, and the time at which the trend becomes significant and stays significant for the remainder of the century is defined as detection time.

Empirical distributions and summary statistics of detection times across the 225 possible time series of differences are then computed and form the basis for our conclusions. A detailed description of the methodology is provided in *SI Text*.

ACKNOWLEDGMENTS. We thank Brian O'Neill, Jean-François Lamarque, two anonymous reviewers, and the editor for their comments and suggestions. C.T. thanks the National Center for Atmospheric Research/Climate and Global Dynamics for hosting her. We acknowledge the modelling groups, the Program for Climate Model Diagnosis and Intercomparison, and the Working Group on Coupled Modelling of the World Climate Research Programme (WCRP) for their roles in making available the WCRP CMIP5 multimodel dataset. Support of this dataset is provided by the Office of Science, US Department of Energy (DOE). Portions of this study were supported by the Office of Science, Biological, and Environmental Research, US DOE (Grant DE-SC0004956) and by the European Commission's Seventh Framework Programme as part of the Earth System Model Bias Reduction and Assessing Abrupt Climate (EMBRACE) project (Grant Agreement 282672).

1. Stocker T, et al. (2013) IPCC 2013: Summary for Policy Makers. *Climate Change 2013: The Physical Science Basis. Contribution of Working Group I to the Fourth Assessment Report of the Intergovernmental Panel on Climate Change* (Cambridge Univ Press, Cambridge, UK and New York).
2. Taylor KE, Stouffer RJ, Meehl GA (2012) A summary of the CMIP5 experiment design. *Bulletin of the American Meteorological Society* 93:485–498.
3. Moss RH, et al. (2010) The next generation of scenarios for climate change research and assessment. *Nature* 463(7282):747–756.
4. van Vuuren DF, et al. (2011) The representative concentration pathways: An overview. *Clim Change* 109:5–31.
5. Meinshausen M, et al. (2011) The RCP greenhouse gas concentrations and their extensions from 1765 to 2300. *Clim Change* 109:213–241.
6. Arora V, et al. (2011) Carbon emission limits required to satisfy future representative concentration pathways of greenhouse gases. *Geophys Res Lett* 38:L05805, 10.1029/2010GL046270.
7. Meehl GA, et al. Climate change projections in CESM1(CAM5). *J Clim* 26:6287–6308.
8. van Vuuren DF, et al. (2011) RCP2.6: Exploring the possibility to keep global mean temperature increase below 2 °C. *Clim Change* 109:95–116.
9. Hegerl GC, et al. (2007) Understanding and attributing climate change. *Climate Change 2007: The Physical Science Basis. Contribution of Working Group I to the Fourth Assessment Report of the Intergovernmental Panel on Climate Change*, eds Solomon S, et al. (Cambridge Univ Press, Cambridge, UK and New York).
10. Mahlstein I, Knutti R, Solomon S, Portman RW (2011) Early onset of significant local warming in low latitude countries. *Environ Res Lett* 6:034009.
11. Hawkins E, Sutton R (2009) The potential to narrow uncertainty in regional climate predictions. *Bulletin of the American Meteorological Society* 90:1095–1107.
12. Hawkins E, Sutton R (2012) Time of emergence of climate signals. *Geophys Res Lett* 39:L01702.
13. Knutti R, et al. (2008) A review of uncertainties in global temperature projections over the twenty-first century. *J Clim* 21:2651–2663.
14. Tebaldi C, Knutti R (2007) The use of the multi-model ensemble in probabilistic climate projections. *Philos Trans A Math Phys Eng Sci* 365(1857):2053–2075.
15. Andrews T, Gregory JM, Webb MJ, Taylor KE (2012) Forcing, feedbacks and climate sensitivity in CMIP5 coupled atmosphere-ocean climate models. *Geophys Res Lett* 39:L09712, 10.1029/2012GL051607.
16. Giorgi P, Jones C, Asrar GR (2009) Addressing climate information needs at the regional level: The CORDEX framework. *World Meteorological Organization Bulletin* 58:175–183.
17. Keeling CD, et al. (1989) A three-dimensional model of atmospheric CO2 transport based on observed winds: 1. Analysis of observational data. *Aspects of Climate Variability in the Pacific and Western Americas*, Geophysical Monograph 55, ed Peterson DH (American Geophysical Union, Washington, DC), pp 165–236.
18. Conway TJ, et al. (1994) Evidence for interannual variability of the carbon cycle from the National Oceanic and Atmospheric Administration/Climate Monitoring and Diagnostics Laboratory Global Air Sampling Network. *J Geophys Res* 99:22831–22855.
19. Anav A, et al. (2013) Evaluating the land and ocean components of the global carbon cycle in the CMIP5 Earth System Models. *J Clim* 26:6801–6843.
20. Giorgi F, Francisco R (2000) Evaluating uncertainties in the prediction of regional climate change. *Geophys Res Lett* 27:1295–1298.
21. Hegerl GC, et al. (2006) Climate change detection and attribution: Beyond mean temperature signals. *J Clim* 19:5058–5077.
22. Hu A, Xu Y, Tebaldi C, Washington WM, Ramanathan V (2013) Mitigation of short lived climate pollutants slows sea level rise. *Nat Clim Chang* 3:730–734.